



GP73 reinforces cytotoxic T-cell function by regulating HIF-1 α and increasing antitumor efficacy

Jialong Liu ^{1,2}, Chao Feng,^{3,4} Ruzhou Zhao,⁵ Hongbin Song,¹ Linfei Huang,⁵ Nan Jiang,⁶ Xiaopan Yang,⁵ Lanlan Liu,¹ Cuijuan Duan,¹ Luming Wan,⁵ Qi Gao,⁷ Lijuan Sun,⁷ Xufeng Hou,⁷ Muyi Liu,⁵ Yanhong Zhang,⁵ Xuemiao Zhang,¹ Dandan Zhang,¹ Yufei Wang,¹ Yong Li,⁸ Xueping Ma,¹ Hui Zhong,⁷ Min Min,⁹ Congwen Wei,⁵ Yuan Cao ³, Xiaoli Yang¹

To cite: Liu J, Feng C, Zhao R, et al. GP73 reinforces cytotoxic T-cell function by regulating HIF-1 α and increasing antitumor efficacy. *Journal for ImmunoTherapy of Cancer* 2025;**13**:e009265. doi:10.1136/jitc-2024-009265

► Additional supplemental material is published online only. To view, please visit the journal online (<https://doi.org/10.1136/jitc-2024-009265>).

Accepted 23 November 2024



© Author(s) (or their employer(s)) 2025. Re-use permitted under CC BY-NC. No commercial re-use. See rights and permissions. Published by BMJ Group.

For numbered affiliations see end of article.

Correspondence to

Xiaoli Yang;
Yangxiaolitw@163.com

ABSTRACT

Background Immunotherapy that targets immune checkpoints has achieved revolutionary success, but its application in solid tumors remains limited, highlighting the need for reliable enhancement of the efficacy of immunotherapy. Golgi protein 73 (GP73), a Golgi membrane protein, has been implicated in various cellular processes, including immune regulation. Recent studies suggested that GP73 may play a role in modulating the immune response in patients with cancer. In this study, we investigated the mechanism by which GP73 regulates T-cell-mediated antitumor immunity within the tumor microenvironment.

Methods We used T-cell specific GP73 knockout mice to establish MC38 and B16 tumor models to investigate the impact of GP73-deficient T cells on tumor growth. Single-cell sequencing was subsequently employed to classify tumor-infiltrating immune cells and assess changes in cytokines and metabolic genes. Through RNA sequencing, real-time quantitative PCR, western blotting, flow cytometry, Seahorse analysis, glucose uptake, and L-lactic acid secretion assays, we explored how GP73 regulates hypoxia-inducible factor 1 α (HIF-1 α) to influence T-cell antitumor functionality. Furthermore, we established adoptive transfer experiments to study the ability of GP73-overexpressing T cells to combat tumors. Blood samples of patient with clinical tumor were collected to assess the relationship between immunotherapy efficacy and T-cell GP73 levels.

Results In this study, the absence of GP73 in mouse T cells promoted tumor growth and metastasis, accompanied by a decrease in the proportion of cytotoxic CD8+T cell subsets infiltrating the tumor and an increase in exhausted CD8+ T-cell subsets. Further analysis revealed that the effector function of CD8+T cells in tumors relies on glycolysis regulated by HIF-1 α rather than immune checkpoints. GP73-deficient T cells exhibit severely impaired glycolysis in hypoxic environments, whereas ectopic GP73 expression restores HIF-1 α levels. In adoptive immunotherapy, overexpression of GP73 in T cells inhibits tumor growth. In cytotoxicity assays, knockdown of GP73 affected the ability of CD8+T cells to kill target cells. Clinically, tumor immunotherapy partial response patients present significantly elevated levels of GP73 expression in T cells.

WHAT IS ALREADY KNOWN ON THIS TOPIC

⇒ Immune checkpoint therapies have been widely applied in clinical tumor treatment. However, this approach exhibits notable limitations in the treatment of solid tumors, particularly characterized by a decline in the cytotoxic capacity of tumor-infiltrating lymphocytes. Golgi protein 73 (GP73), a Golgi membrane protein, has been demonstrated to be involved in various tumor processes through its participation in immune regulation. Here, we observed that GP73 was upregulated in T cells of tumor microenvironment and involved in glycolysis. Further in-depth exploration is needed regarding the impact of GP73 on T-cell function and its implications for tumor immunotherapy.

WHAT THIS STUDY ADDS

⇒ In this study, we developed a T-cell GP73-deficient mouse model, aiming to explore the potential of targeting GP73 to enhance tumor immunotherapy. The data indicated that the absence of GP73 inhibits the antitumor capability of T cells, primarily due to restricted hypoxia-inducible factor 1 α (HIF-1 α)-driven glycolysis. Ectopic expression of GP73 and HIF-1 α in T cells can restore T-cell cytotoxicity and glycolysis. Clinical findings showed that GP73 levels are significantly elevated in the T cells of patients with lung cancer who exhibit a partial response to PD-1 antibody therapy, consistent with our preliminary experimental results.

HOW THIS STUDY MIGHT AFFECT RESEARCH, PRACTICE OR POLICY

⇒ The results of this study suggested that GP73 is a potential biomarker for predicting clinical responses to tumor immunotherapy and plays a critical role in the antitumor efficacy of CD8+T cells. Targeting GP73 may provide a novel strategy to enhance the effectiveness of tumor immunotherapy.

Conclusions These findings reveal the role of GP73 in regulating T-cell glycolysis and may lead to new therapeutic strategies for the prognosis and treatment of clinical tumor immunotherapy.

INTRODUCTION

The rapid development of tumor immunotherapy has led to new strategies for tumor treatment. Current immunotherapeutic approaches included enhancing the infiltration of endogenous tumor-infiltrating lymphocytes (TILs) through checkpoint blockade or transferring autologous T cells modified with chimeric antigen receptors (CAR-modified) into patients.^{1,2} However, a significant proportion of patients, especially those with solid tumors, did not benefit from these treatments.³ The activity of TILs was often used to assess the effectiveness of antitumor immunotherapy.⁴ Dysfunctional TILs exhibited changes at the transcriptional level, leading to the inhibition of their survival and effector functions and the promotion of immune escape by tumors. Therefore, immunotherapy targeting solid tumors required the identification of other mechanisms driving T-cell dysfunction to rescue the effector functions of TILs.

The solid tumor microenvironment (TME) was characterized by hypoxia and involves immunosuppressive myeloid cells and regulatory T cells.⁵ Tumor hypoxia was a hallmark of invasive malignancies and promotes immune evasion by recruiting immunosuppressive cells.^{6,7} T cells were affected by hypoxic conditions in terms of development, differentiation, maturation, migration, and function.^{8,9} One way in which T cells adapted to hypoxia is by regulating metabolic activities, with a key player being hypoxia-inducible factor 1 α (HIF-1 α).¹⁰ HIF-1 α -mediated glycolysis enabled cells to adapt to low-oxygen conditions, underscoring the importance of HIF-1 α in T-cell function within the hypoxic tissue microenvironment.

The expression of HIF-1 α in T cells can be induced through both hypoxic and non-hypoxic pathways, including T-cell receptor (TCR) triggering and PI3K-mediated pathways, leading to mRNA upregulation and protein stabilization.^{11,12} Hypoxia can directly enhance the effector function of CD8+T cells.¹³ Recent studies have revealed the role of HIF-1 α in regulating T-cell effector function, exhaustion, and memory differentiation in malignant tumors.¹⁴ HIF-1 α was crucial for shifting T-cell metabolism toward glycolysis during TCR activation, promoting the proliferation and effector function of T cells.^{15,16} In a mouse melanoma model, CD8+T cells with HIF-1 α deficiency exhibited decreased antitumor activity, whereas CD8+T cells with Von Hippel-Lindau (VHL) deficiency, which play a critical role in controlling the stability of HIF-1 α , showed enhanced control of tumor growth.^{14,17} These findings suggested a critical role for HIF-1 α in regulating T-cell responses to malignant tumors, although the exact underlying mechanisms remain unclear.

Golgi protein 73 (GP73), also known as GOLM1 or Golph2, is a Golgi type II transmembrane protein that is differentially expressed across tissues.¹⁸ GP73 was recognized as an oncogenic protein in various malignancies, including hepatocellular carcinoma (HCC), prostate cancer, lung cancer, renal cancer, and glioblastoma.^{19–21} Recent studies have indicated that tumor cell expressed

GP73 influences the TME and tumor immunity.²² GP73 functions as a positive regulator of PD-L1 expression through the EGFR/STAT3 signaling pathway in human HCC cells.²³ We also discovered that GP73 regulates the TME by inducing endoplasmic reticulum (ER) stress in tumor-associated macrophages (TAMs) and suppressing CD8+T cells.²⁴ Additionally, GP73 overexpression in HCC cells was associated with an immunosuppressive microenvironment, promoting PD-L1 stabilization and transporting PD-L1 into TAMs, leading to CD8+ T-cell suppression.²⁵ Our previous study suggested that GP73 acts as a gluconeogenic hormone, possesses Rab GTPase-activating protein activity, and affects apolipoprotein B secretion.²⁶ However, limited data exist regarding the role of T cells expressing GP73 in antitumor immunity.

In this study, we discovered a positive correlation between GP73 and T-cell activation. Moreover, the growth of subcutaneous MC38 tumors was accelerated in T-cell specific GP73 knockout mice (hereafter, GP73^{fl/fl}), and the lung metastasis of B16-F10 melanoma cells was promoted. Single-cell RNA sequencing of tumor-infiltrating immune cells from GP73^{fl/fl} mice revealed a decrease in the proportion of cytotoxic CD8+T cells and an increase in the proportion of exhausted CD8+T cells. Importantly, this depletion did not depend on changes in immune checkpoint molecules but rather is due to defects in glycolysis. Therefore, the expression of GP73 was crucial for T-cell effector responses in the TME. Further investigation revealed that HIF-1 α is the downstream of GP73, and GP73-deficient T cells presented reduced the expression of HIF-1 α and other glycolysis-related genes. Cellular energy respiration experiments demonstrated a significant decrease in glycolysis in GP73-deficient T cells. We developed lentiviral vectors for ectopic GP73 expression to increase the cytolytic function of CD8+T cells in vitro and in xenograft models and to restore HIF-1 α expression and glycolytic capacity in GP73-deficient T cells. Additionally, our results revealed that mammalian target of rapamycin (mTOR) agonists could induce the activation of ECAR in GP73-deficient T cells. Therefore, we proposed that the absence of GP73 in T cells may inhibit HIF-1 α -driven glycolysis by reducing mTOR activity. Finally, clinical research revealed elevated GP73 in the T cells of patients with solid tumor in response to immunotherapy, which was consistent with the aforementioned experimental findings. These studies revealed that GP73 is a potential biomarker for predicting the clinical response to immunotherapy and plays a crucial role in the antitumor efficacy of CD8+T cells. Targeting GP73 may offer a novel strategy to increase the effectiveness of tumor immunotherapy.

MATERIALS AND METHODS

Reagents

DMEM/high glucose (03.1002C), RPMI-1640 (03.4007C), and penicillin–streptomycin solution (03.12001A) were purchased from Eallbio. Fetal bovine serum (35-081-CV)

was purchased from Corning. The EasySep Human T-cell Isolation Kit (17951C), EasySep Mouse T-Cell Isolation Kit (19851A), EasySep Mouse CD8+TCell Isolation Kit (19853), and EasySep Magnet (18000) were purchased from Stemcell. Red blood cell lysis buffer (R1010), Triquick reagent (TRIzol Substitute; R1100), collagenase IV (C8160), the Annexin V-FITC Apoptosis Detection Kit (CA1020), trifluoromethoxy carbonylcyanide phenylhydrazide (FCCP; IF0690), oligomycin A (IO0460), and lymphocyte separation medium (Human, P8610; Mouse, P8620) were purchased from Solarbio. MHY1485 (S7811) was purchased from MCE. Pierce Rapid Gold BCA (A53225) was purchased from Thermo Fisher Scientific.

Antibodies

Anti- β -actin (81115-1-RR, 1:5000 dilution), anti-GAPDH (60004-1-Ig, 1:10000 dilution), anti-GP73 (15126-1-AP, 1:2000 dilution), anti-mTOR (66888-1-Ig, 1:5000 dilution), and anti-P-mTOR (67778-1-Ig, 1:2500 dilution) antibodies were purchased from Proteintech. Anti-HIF-1 α (ab179483, 1:2000 dilution) antibody was purchased from Abcam. The anti- β -tubulin (AC030, 1:10000 dilution) antibody was purchased from ABclonal. Alexa Fluor 700 anti-human CD11b (301356), PerCP/Cyanine5.5 anti-human CD3 (317336), FITC anti-human CD45 (304006), APC/Cyanine7 anti-human CD15 (323048), Ultra-LEAF purified anti-mouse CD3 (100238), Ultra-LEAF purified anti-mouse CD28 (102116), purified anti-human CD3 (317302), and purified anti-human CD28 (302902) antibodies were purchased from Biolegend. PE-conjugated anti-human GOLPH2 (MA5-40951), PE-Cyanine7-conjugated anti-human CD14 (25-0149-42), PerCP-eFluor 710-conjugated anti-human CD16 (46-0166-42), Alexa Fluor700-conjugated anti-human CD8a (56-0086-42), PE-Cyanine7-conjugated anti-human CD4 (25-0049-42), APC-conjugated anti-human IFN- γ (17-7319-82) and PE-conjugated anti-human Granzyme B (12-8896-42) antibodies were purchased from Thermo Fisher Scientific.

Construction of the overexpression plasmid

The GP73-overexpressing lentivirus was constructed by Genechem Co. (Shanghai, China), the sequence of GP73 was obtained from NCBI and then subcloned and inserted into a lentiviral vector to overexpress GP73; the empty vector was used as a negative control. The cells were transfected with lentivirus three times, with each period lasting for 48 hours; then, immunoblot was used to assess the efficiency of GP73 overexpression.

Cell culture

The MC38 (SAC0538) cell line was obtained from AoYinbio Cell Center. The Lewis lung carcinoma (LLC, CL-0140) cell line was obtained from Procell Life Science & Technology Co. The MC38-OVA (CTCC-001-0648) and B16-F10 (CTCC-400-0304) cell lines were obtained from Zhejiang Meisen Cell Technology Co. MC38, MC38-OVA and LLC cells were incubated in DMEM, while B16-F10

was incubated in RPMI-1640. All the cells were cultured at 37°C in a humidified atmosphere with 5% CO₂.

Clinical sample collection and preparation

Eight healthy donors and eight patients with pathologically diagnosed cancer, including three patients with HCC, three patients with colorectal cancer and two patients with pancreatic cancer, and GP73 expression levels in T cells of the above participants were tested.

To investigate the differences in GP73 levels in T cells from patients with stable disease and partial response to tumor immunotherapy, we collected a total of 21 samples. Detailed information about the 21 patients is provided in online supplemental table S1.

All clinical samples were collected from The General Hospital of the People's Liberation Army. This study was approved by the Ethics Committee of the Chinese PLA General Hospital (KY2021-009-01). All patients signed the informed consent form in person.

Animals

C57BL/6J and OT-1 mice were purchased from SPF biotech Co (Beijing, China). The mice were housed in a pathogen-free environment with controlled temperature, following a 12 hours light and dark cycle. The temperature was maintained between 21°C and 23°C, with relative humidity set at 50%–60%. They had unrestricted access to food and water at the Academy of Military Medical Sciences (AMMS) Animal Center (Beijing, China). Prior to any procedures, the mice were group-housed for 3 days. All animal experiments were performed at the AMMS Animal Center (approved animal protocol number IACUC-DWZX-2023-P022), ensuring compliance with all relevant ethical guidelines for the use of research animals.

To generate GP73^{fl/fl} mice, we crossed loxP-flanked allele mice with dLck or Tie2-Cre mice to delete the loxP-flanked genes in T cells. This produced mice with homozygous loxP-flanked alleles without Cre (hereafter, WT) or hemizygous alleles for Cre (recorded as GP73^{fl/fl}).

For construction of the mouse tumor models, 1×10⁶ MC38 or LLC cells were subcutaneously injected into each mouse, while 5×10⁵ B16-F10 cells were injected. The tumor volume was estimated by the formula $a^2 \times b \times 0.5$, where b was the tumor larger dimension. Tumors were isolated and weighed after the mice were sacrificed.

T-cell isolation

Human peripheral blood T cells were isolated via a human CD3+ T-cell isolation kit (BEAVER, 71003-100). For mouse CD3+ and CD8+ T cells, corresponding isolation kits were used (BEAVER, 70903-100; 70902-100). Briefly, after the spleen was ground, the spleen homogenate was filtered through a 100 μ m filter and washed twice with 1×PBS. Sorting was subsequently performed according to the kit instructions.

T-cell proliferation assay

A CCK8 kit (Beyotime, C0037) was used to assess T-cell proliferation. In brief, T cells were activated and cultured

for 0, 3, 5, or 7 days, and the absorbance at 450 nm was measured for each well. The specific methodology followed the manufacturer's instructions.

T-cell adoptive therapy

MC38-OVA cells (2×10^6) were injected subcutaneously into C57BL/6J mice, and purified CD8+T cells from OT-1 mice were activated for 72 hours with plate-bound anti-CD3 (5 µg/mL) and soluble anti-CD28 (3 µg/mL) antibodies. Activated T cells were further infected with pCDH-vector and pCDH-GP73 viruses, and on day 8 post-tumor implantation, they were injected into mice via tail vein injection (2×10^6). Tumor size was subsequently monitored.

In vitro cytotoxic T-cell killing assay

The release of lactate dehydrogenase (LDH) into the cell culture supernatant was assessed by using an LDH Cytotoxicity Assay Kit (Beyotime, C0016). Briefly, MC38-OVA cells were incubated in a 96-well plate (2×10^4 cells) for 6 hours to allow adherence. CD8+T cells from OT-1 mice were activated, allowed to proliferate for 3 days, and then added to MC38-OVA wells at a 3:1 ratio for coculture.²⁷ Microscopy images were taken after 1 and 6 hours of coculture, and the supernatant from the 6-hour culture was collected for LDH level detection. The maximum LDH release control was achieved by adding 1% Triton X-100, and the LDH release (%) was calculated according to the manufacturer's instructions. The levels of IFN-γ and TNF-α in the cell supernatant were measured using the Luminex xMAP technology by LAIZEE Biotech Co (Shanghai, China), while the GZMB levels were detected using an ELISA kit (LAIZEE, LEM923-2).

Quantitative real-time PCR

Total mRNA was extracted from cells via NucleoZOL, cDNA synthesis was performed according to the manufacturer's instructions (TransGen, AT311-03), the relative levels of individual mRNAs were calculated after normalization to the β-actin in the corresponding sample as previously described. The primer sequences used are shown in online supplemental table S2.

Immunoblot

T cells were lysed in cell lysis buffer (Beyotime, P0013) supplemented with fresh protease inhibitors after treatment. Whole-cell lysates were subjected to SDS-PAGE, transferred to PVDF membranes, and analyzed by immunoblotting with the indicated primary antibodies.

Flow cytometry

Single-cell suspensions were prepared from human peripheral blood and mouse tumors. Immune cells and cytokine expression were determined via intracellular staining. For TNF-α, IFN-γ and Granzyme B (GZMB) intracellular staining, T cells were activated for 12 hours in the presence of protein transport inhibitor (BD, 554724) and then fixed and permeabilized with 4% formaldehyde (without methanol) and 0.2% Triton X-100

before intracellular staining. Immunophenotyping was performed via Thermo Fisher Attune NxT, and the data were analyzed via FlowJo V.10.8.1.

Single-cell sequencing

Preprocessing, filtering, normalization, integration and clustering

The 'Seurat' R package (V.4.3.0) was used for quality control procedures and subsequent bioinformatic analyses. To eliminate doublets, we employed the R package DoubletFinder²⁸ with a permissive assumption, specifically, a 3% doublet rate. We removed low-quality cells on the basis of the following criteria: a threshold of UMIs below 500 or exceeding 10 000, as well as a mitochondrial gene count proportion surpassing 25%. Following these quality control measures, we executed a sequence of preprocessing steps for downstream analysis. More precisely, we engaged in a global scaling normalization known as 'log normalization', which harmonized the expression of features across each cell, multiplying the cumulative expression by a default scaling factor of 10 000. We subsequently logarithmically transformed the results via the 'NormalizeData' function in Seurat. Highly variable genes were determined via the Seurat function 'FindVariableGenes'. Next, we consolidated the normalized expression profiles from all samples via the 'merge' function in R (V.4.2.3). To discern shared cell states spanning different datasets, we initially integrated these datasets by leveraging harmony²⁹ (V.0.1.0), which was meticulously crafted to mitigate the influence of technical artifacts across datasets and cells. After this, we applied the 'FindNeighbors' and 'FindClusters' functions in the Seurat R package to cluster the cells. Specifically, the 'FindNeighbors' function identifies each cell's nearest neighbors by calculating the similarity between cells and builds a nearest neighbor graph. On the basis of the graph, we employed the Louvain algorithm in the 'FindClusters' function for cell clustering. To determine the appropriate number of clusters, we conducted a resolution parameter sweep by setting the resolution parameter in the FindClusters function to 0.2, 0.4, 0.6, 0.8, 1.0, and 1.2 and evaluated the clustering results on the basis of several criteria, including cluster stability, biological relevance, and distinct marker gene expression patterns.

Cell type annotation

We calculated the T-cell function gene module score via the 'AddModuleScore' function in Seurat. The functional gene sets were adapted from Chu *et al.*³⁰ (online supplemental table S3). The cell type markers used were adapted from Feng *et al.*³¹

Differential gene expression analysis

The marker genes in each subcluster were identified through the 'FindAllMarkers()' function in Seurat with the default parameters. Differentially expressed genes (DEGs) between the wild-type (WT) and knockout (GP73^{fl/fl}) groups were ascertained through the Wilcoxon rank-sum test, accompanied by Bonferroni correction,

contingent on the following criteria: (1) expression in more than 20% of cells within either or both groups, (2) $|\log_2\text{FC}| > 0.5$, and (3) Wilcoxon rank-sum test adjusted p value < 0.01 .

RNA sequencing

Gene expression levels were quantified as fragments per kilobase of transcript per million mapped reads (FPKM). Due to the limited number of samples (three per group), upregulated or downregulated genes in the tumor cells were identified based on a greater than or equal to twofold change in expression to assess overall differences. Gene set enrichment analysis (GSEA) was employed to investigate the differences in molecular signaling pathways between tumors from WT and GP73^{fl/fl} mice to assess the variations in tumor growth status. The RNA sequencing of tumor samples was conducted by Shanghai biotech Co.

Seahorse

Metabolic analysis was carried out via an Extracellular Flux Analyzer XFe24 (Agilent). Spleen T cells were isolated via T-cell isolation kits (purity $\geq 95\%$) according to the manufacturer's protocols. Briefly, activated T cells (5×10^5) were transferred to a Cell-Tak (Corning, 354240)-coated Cell Culture Microplate (Agilent, 100777-004), and the plate was centrifuged at $400 \times g$ for 5 min to accumulate cells at the bottom. At 37°C in a CO_2 -free incubator, the plate was incubated for 1 h before being transferred to the seahorse machine for metabolic analysis. Glycolytic rate and mitochondrial stress were measured via the extracellular acidification rate (ECAR) (mpH/min) and oxygen consumption rate (OCR) (pmoles/min), respectively, via real-time injection. For the ECAR analysis, the cells were resuspended in XF assay medium (non-buffered RPMI base medium, 25 mM glucose, 2 mM glutamine and 1 mM sodium pyruvate) with injections of rotenone and antimycin (Rot/AA; both 5 μM ; Sigma Aldrich Corporation, R8875 and A8674) and 2-deoxy-D-glucose (2-DG, 100 mM; Sigma Aldrich Corporation, D8375-5G). For the OCR analysis, the cells were resuspended in XF assay medium and treated with oligomycin (Oligo; 1 μM ; Sigma Aldrich Corporation, 75351-5 MG), trifluoromethoxy carbonylcyanide phenylhydrazine (FCCP; 10 μM ; Sigma Aldrich Corporation, C2920-10 MG) and Rot/AA (both 5 μM). The OCR and ECAR values were calculated via the program provided by the manufacturer, and the data files were exported as excel files.

Glucose uptake assay

After T-cell activation, the cells were washed twice with $1 \times \text{PBS}$, resuspended and incubated overnight in sugar-free medium containing 10% FBS. Then, 2-NBDG (100 μM) was added to the medium, and the mixture was incubated under hypoxic conditions (1% O_2) for 30 or 60 min. After incubation, the cells were collected, washed twice with $1 \times \text{PBS}$, and subsequently analyzed via a flow cytometer equipped with FlowJo software.

L-lactic acid secretion assay

After isolation from the spleen, T cells (1×10^6 per well) were cultured and activated for 3 days and then cultured for 24 hours under 21% or 1% oxygen. The medium supernatant was collected to detect the L-lactic acid content following the manufacturer's protocol.

Statistical analysis

Unpaired Student's t -tests were used for two-group comparisons, survival data were evaluated with the log-rank (Mantel-Cox) test, and grouped data were analyzed via two-way analysis of variance (ANOVA), with subsequent Sidak correction for the adjustment of multiple comparisons. Significance was defined as a $p \leq 0.05$. No data-point exclusion criteria were employed, and the assessment of data distribution normality and variance was omitted.

RESULTS

GP73 is upregulated in activated T cells

To study the expression of GP73 in T cells, we examined the expression of GP73 in resting and activated mouse T cells obtained from WT mice. Our results showed that GP73 is detectable in T cells, and its expression increased over time with activation (figure 1A–C). A similar trend was observed for T cells isolated from healthy individuals (figure 1D–F). These findings strongly suggested that GP73 is swiftly upregulated in response to T-cell activation. With these insights, we sought to investigate whether GP73 plays a cell-autonomous role in T cells.

Genetic deletion of GP73 in T cells accelerates tumor growth

To study the effects of GP73 on T cells, we inserted loxP flanking sequences at both ends of the GP73 allele and subsequently expressed Cre under the control of the lymphocyte protein tyrosine kinase (LCK) promoter. This allowed for the thymocyte-specific excision of the loxP flanking sequences, thereby leading to the deletion of GP73 in T cells (recorded as GP73^{fl/fl}). This strategy completely suppressed GP73 expression in T cells (online supplemental figure S1), and had no effect on T-cell proliferation (online supplemental figure S1B). To elucidate the role of the GP73 pathway in T cells during tumor growth, we conducted a comprehensive study employing three distinct C57BL/6J mouse tumor models with varying immunogenicities. The corresponding tumor cells were subcutaneously inoculated into both WT and GP73^{fl/fl} littermate control mice, and tumor growth was recorded. The tumor models included highly immunogenic orthotopic MC38 colon tumor cells, moderately immunogenic B16-F10 melanoma tumor cells, and poorly immunogenic LLC cells. Our study revealed that MC38 tumor cells exhibited faster growth in GP73^{fl/fl} mice (figure 2A), with a significantly increased tumor burden observed at the 14-day endpoint (figure 2B). Similarly, B16-F10 tumor cells exhibited a moderate increase in growth rate and tumor volume at the endpoint of day 10 (figure 2D), with a significant increase in tumor burden observed by day 13

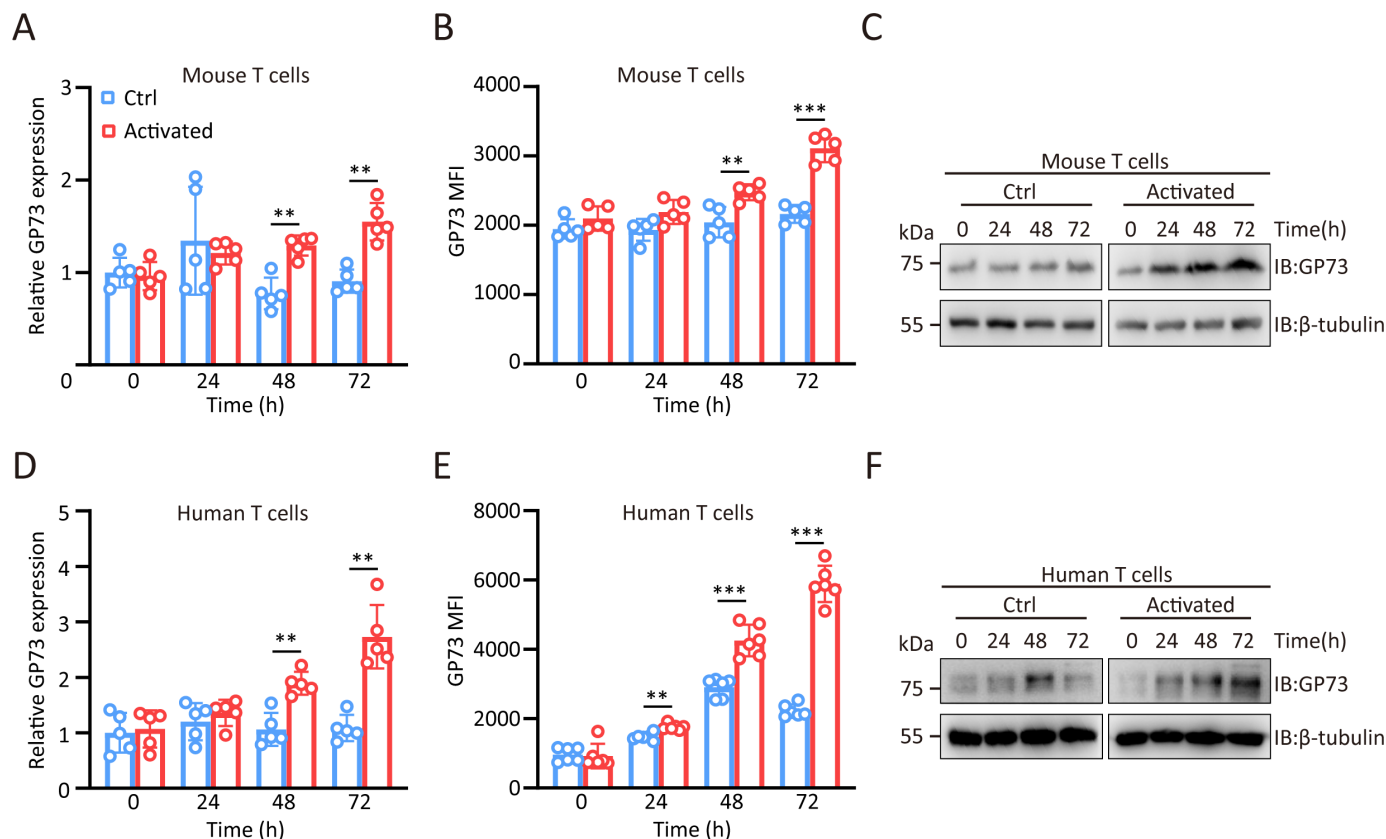


Figure 1 The activation of T cell promotes GP73 expression. (A) qRT-PCR of relative mRNA levels of GP73 on magnetically isolated mouse spleen T cells before and after activation with CD3/CD28 antibody and IL-2 for the indicated time points (n=5). (B) The MFI of intracellular GP73 in activated splenic T cells from mice, measured after specific activation times (n=5). (C) Immunoblots showing GP73 expression in mouse spleen T cells. (D) qRT-PCR of relative mRNA levels of GP73 on magnetically isolated human peripheral blood T cells before and after activation with CD3/CD28 antibody and IL-2 for the indicated time points (n=5). (E) Intracellular MFI of GP73 in human peripheral blood T cells activation for the indicated time points (n=6). (F) Immunoblots showing GP73 expression in human peripheral blood T cells. Grouped data were assessed by two-way ANOVA for multiple comparisons with Sidak correction; *** $p < 0.001$, ** $p < 0.01$, * $p < 0.05$; ANOVA, analysis of variance; GP73, Golgi protein 73; ns, not significant.

(figure 2E). Furthermore, the ability of melanoma cells to metastasize to the lungs was enhanced in GP73^{fl/fl} mice (figure 2G–H). However, the ability of GP73-deficient T cells to control tumor growth was impaired, leading to decreased survival (figure 2C, F). Interestingly, although the tumor burden caused by LLC tumor cells did not differ between the two groups of mice (online supplemental figure S1C, D), slightly accelerated mortality in GP73^{fl/fl} mice (online supplemental figure S1E). Considering the pivotal role of macrophages in tumor immunity, we generated GP73 macrophage-specific deletion mice (Lyz2^{Cre+}GP73^{fl/fl}) in which the level of GP73 in macrophages was demonstrated (online supplemental figure S1F). Intriguingly, our observations indicated that the deletion of GP73 in macrophages did not influence tumor growth compared with that in littermate control mice (online supplemental figure S1G, H). The isolated MC38 tumors were subsequently analyzed via RNA sequencing, and functional enrichment analysis and genomic enrichment analysis were subsequently performed via the Kyoto Encyclopedia of Genes and Genomes (KEGG) database (online supplemental figure S2A). GSEA revealed that

hypoxia and epithelial–mesenchymal transition signaling pathways were highly expressed in MC38 tumors in GP73^{fl/fl} mice, suggesting that the TME was more conducive to tumor growth and metastasis (online supplemental figure S2B, C). Collectively, GP73 played an important intrinsic role in regulating the antitumor activity of T cells.

Genetic deletion of GP73 did not affect the T-cell composition ratio

To further examine the composition and phenotype of tumor-infiltrating immune cells in the TME and the role that GP73 plays in T cells, we harnessed the capabilities of 10×Genomics single-cell RNA sequencing (scRNA-seq) technology. Fourteen days after MC38 tumor injection, we isolated CD45+ immune cells from tumors via CD45+ magnetic beads and subjected them to scRNA-seq (figure 3A). This effort yielded data from a total of 27969 cells through scRNA-seq. After filtering out low-quality cells, 24574 cells (11551 from WT and 13023 from GP73^{fl/fl} mice) were retained for further analysis. The cells in all samples were normalized and integrated for a systematic analysis of immune-cell

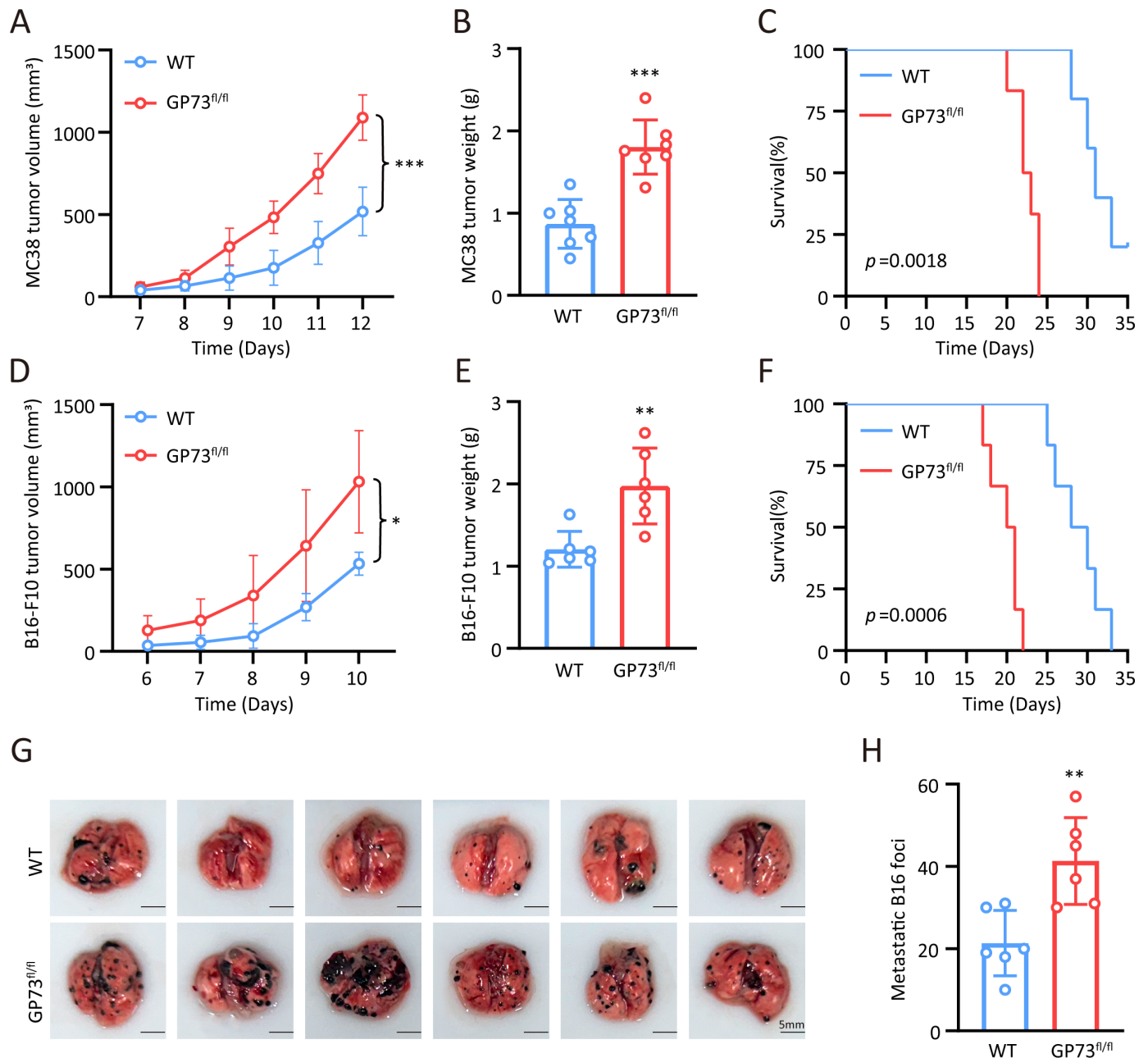


Figure 2 GP73-deficient T cells exhibit reduced tumor growth inhibition capability. (A) Growth curves of subcutaneous MC38 tumors (1×10⁶ cells per mouse) in WT (blue) and GP73^{fl/fl} (red) (n=7 per group). Statistical analysis was performed by two-way ANOVA with Sidak correction for multiple comparisons. Tumor volumes are shown (mean values±SD). (B) MC38 tumor weights on day 14 of the experiment (error bars represent SD). (C) Overall per cent survival of the experiment. Statistical analysis by log-rank (Mantel-Cox) test (n=6). (D) Growth curves of subcutaneous B16-F10 tumors (1×10⁵ cells per mouse) in WT (blue) and GP73^{fl/fl} (red) (n=6 per group). Statistical analysis was performed by two-way ANOVA with Sidak correction for multiple comparisons. Tumor volumes are shown (mean values±SD). (E) B16-F10 tumor weights on day 13 of the experiment (error bars represent SD). (F) Overall per cent survival of the experiment. Statistical analysis by log-rank (Mantel-Cox) test (n=6). (G) Images of lung metastases from B16-F10 melanoma in mice (n=6). (H) Quantitative analysis of melanoma metastases (n=6, error bars represent SD). ***p<0.001, **p<0.01, *p<0.05; ANOVA, analysis of variance; GP73, Golgi protein 73; ns, not significant; WT, wildtype.

populations. We applied graph-based clustering techniques to identify populations and employed uniform manifold approximation and projection for visualization (figure 3B). On the basis of the results from the ScType³² and the expression of marker genes, all the cells were categorized as CD8⁺T cells, CD4⁺ T cells, NK

cells, B cells or macrophages (figure 3B). Further analysis involved differential expression assessments between clusters, which revealed distinctive gene signatures, offering compelling evidence for the unique molecular characteristics defining each cluster's identity. To corroborate the algorithm-assisted identification of cell clusters,

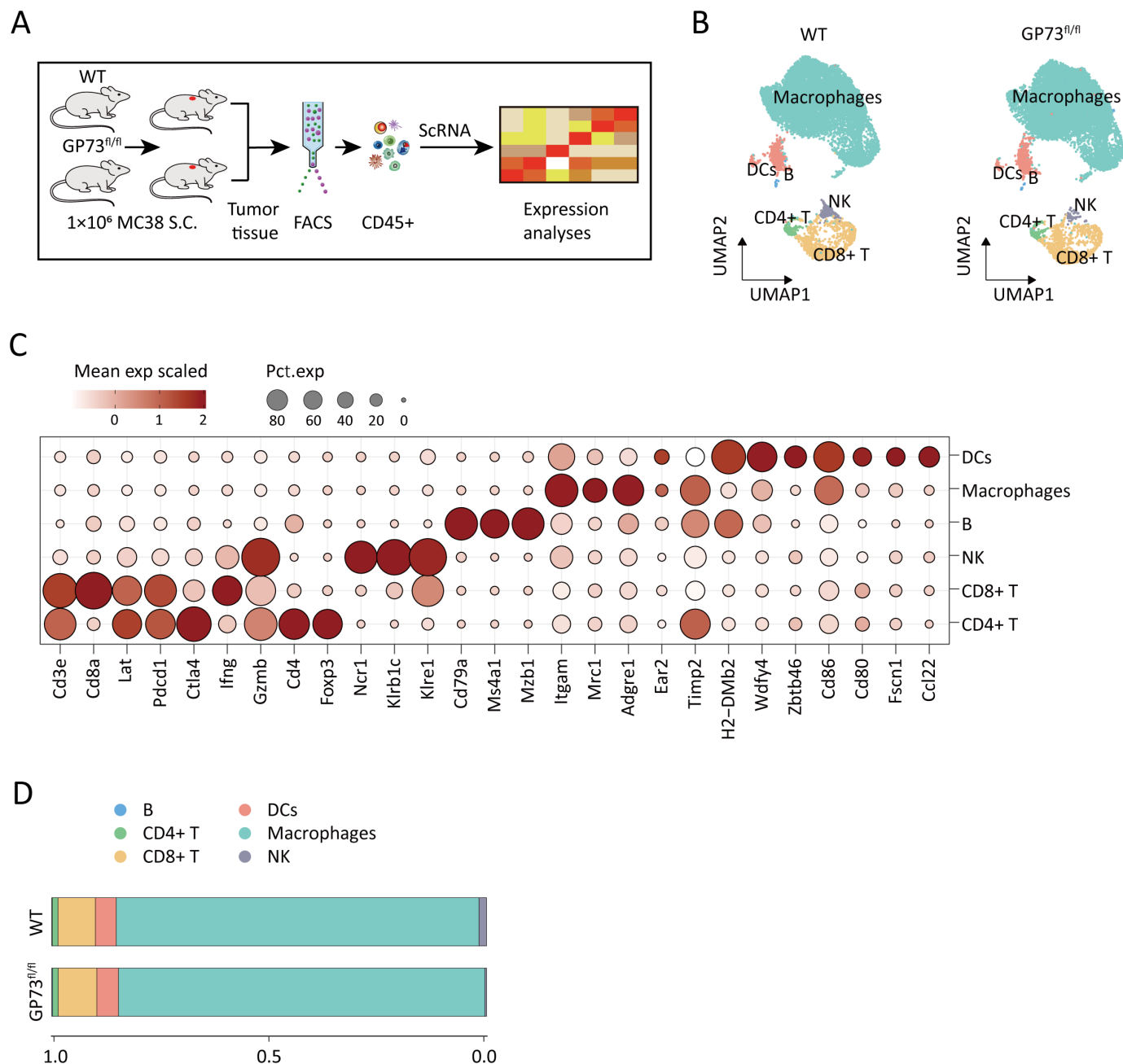


Figure 3 The proportion of tumor-infiltrating T cells was not affected by GP73 deletion. (A) Schematic of the experimental design for scRNA-seq. After 14 days of subcutaneous MC38 tumors (1×10⁶ cells per mouse) in WT and GP73^{fl/fl}, all the mice were sacrificed for isolating tumor-infiltrated CD45+ cells, which were used to scRNA-seq. (B) UMAP plots of single-cell transcriptomic profiles from WT and GP73^{fl/fl} tumor-infiltrated CD45+ cells and divided into 6 clusters. (C) Marker gene expression across defined CD45+ cell clusters. Bubble size is proportional to the percentage of cells expressing a gene and color intensity is proportional to average scaled gene expression. (D) Barplots depicting percentage of cells projected in each CD45+ cell subtype for the indicated conditions. GP73, Golgi protein 73; scRNA-seq, single-cell RNA sequencing; UMAP, uniform manifold approximation and projection; DCs, dendritic cells; FACS: fluorescence activated cell sorter; WT, wildtype.

we scrutinized the expression of well-established cellular markers within our dataset. As anticipated, the expression of these markers aligned with the respective cluster identities (figure 3C). Notably, a significant overlap in gene expression profiles was observed among closely related cell clusters. These findings underscored the necessity of adopting a multidimensional analytical approach to comprehensively delineate cellular heterogeneity within

the TME, and they suggested that lymphoid and myeloid cell subpopulations within the TME exhibit distinct molecular attributes. After these cell clusters were identified, we analyzed the differences between WT and GP73^{fl/fl} tumor-infiltrating immune cells. Our analysis revealed no significant differences in the CD8+ or CD4+ T-cell clusters between the two groups (figure 3D). Intriguingly, we noted a reduction in NK cell levels in GP73^{fl/fl}

tumors (figure 3D). In conclusion, knocking down GP73 in T cells did not affect the proportions of CD8+ T cells or CD4+ T cells among tumor-infiltrating immune cells, and these results prompted us to further analyze each T-cell subpopulation.

Genetic deletion of GP73 reduces the cytotoxicity of CD8+ T cells

To further investigate the cellular subsets of tumor-infiltrating T cells, we conducted an in-depth analysis focused on infiltrating CD8+ T cells to explore the impact of GP73 deficiency on CD8+ T-cell phenotypes. To gain a clearer understanding of the status of CD8+ T cells, we reclassified these cells from both the WT and GP73^{fl/fl} samples into 10 distinct clusters (figure 4A) via an unsupervised clustering approach, the details of which are described in the Materials and methods section. Using differential gene expression and gene signatures sourced from a previous study and established immunomarkers,³⁰ we defined 10 unique transcriptional states for CD8+ T cells: 'naïve-like' (Tn, C6), 'exhausted' (Tex, C3, C4, C7, C9), 'cytotoxic' (Tctl, C1), 'stress response' (Tstr, C0, C2, C8), and 'other' (Tun, C5) CD8+ T cells (figure 4B, C). Compared with those in the WT group, we observed a relative reduction in the proportions of cytotoxic (WT: 18.5%, GP73^{fl/fl}: 11.1%) and stress response (WT: 30.2%, GP73^{fl/fl}: 23.0%) CD8+ T cells, whereas the proportion of exhausted CD8+ T cells (WT: 31.3%, GP73^{fl/fl}: 47.3%) appeared to increase (figure 4D). Our analysis revealed that, in comparison with that in the WT group, the cytotoxicity of Tctl did not significantly change, whereas the cytotoxicity of Tex and Tstr notably decreased (figure 4E). Importantly, there was no significant difference in exhaustion across all T-cell types (figure 4F). To validate the above results, we isolated and analyzed tumor-infiltrating T cells from MC38 tumors. Flow cytometry was used to determine the proportions of CD4+ and CD8+ T cells (online supplemental figure S3A), as well as the expression levels of GZMB and IFN- γ . Additionally, to investigate the exhaustion status of tumor-infiltrating T cells, we measured the expression of immune checkpoint receptors, including PD-1, LAG3, TIGIT, and TIM3. Consistent with the above results, the proportions of MC38 tumor-infiltrating CD4+ T cells and CD8+ T cells did not change (figure 4G–H), and the protein expression (online supplemental figure S3B) and transcriptional levels (online supplemental figure S3C–F) of the immune checkpoints PD-1, LAG3, TIGIT, and TIM3 did not significantly change. However, GP73-deficient tumor-infiltrating CD8+ T cells presented a reduction in the expression of effector molecules such as GZMB and IFN- γ (figure 4I, J), suggesting that GP73-deficient CD8+ T cells have reduced cytotoxicity. Notably, our results showed that the reduction in cytotoxicity in GP73-deficient CD8+ T cells was not dependent on changes in immune checkpoints, and we further explored the mechanisms that affect CD8+ T-cell cytotoxicity.

Reduced expression of HIF-1 α in GP73-deficient CD8+ T cells

To explore the mechanism underlying the cytotoxicity of tumor-infiltrating CD8+ T cells, we performed a comprehensive analysis of single-cell sequencing data to identify DEGs and altered signaling pathways in distinct subsets of GP73-deficient CD8+ T cells. We observed decreased expression of HIF-1 α in CD8+ T cells and in each subset, except for the Tn subset (figure 5A). In addition, our analysis revealed a marked downregulation of genes related to cytotoxicity in Tstr and Tex from GP73^{fl/fl} (figure 5B). Furthermore, we detected significant changes in the expression of genes associated with hypoxia signaling pathways and glycolysis signaling pathways within the Tctl, Tex and Tstr cell clusters (figure 5C–E). Subsequent GSEA of the DEGs revealed that hypoxia-related and glycolysis-related genes were more prominently enriched in CD8+ T cells from WT mice, particularly in the Tctl, Tex and Tstr subgroups (figure 5F–H). Moreover, we observed a similar decrease in the glycolytic score in the GP73 deletion group, especially in the Tex, Tstr and Tun subgroups (figure 5I). Given that HIF-1 α is a key factor in glycolysis, these findings suggest a decrease in glycolytic levels in the CD8+ T-cell subpopulations of GP73^{fl/fl} mice due to HIF-1 α loss. These results suggest that the reduction in the proportion of cytotoxic T cells observed in GP73^{fl/fl} mice may be attributed to the downregulation of HIF-1 α expression in CD8+ T cells.

Genetic deletion of GP73 reduces the glycolytic capacity of T cells

To investigate the mechanism by which GP73 affects HIF-1 α , we cultured extracted mouse splenic T cells in a hypoxic environment. Our immunoblotting (figure 6A) and qRT-PCR (figure 6B, C) results indicated that the expression of GP73 and HIF-1 α was continuously upregulated under hypoxic conditions. Intriguingly, we observed that HIF-1 α in GP73-deficient T cells did not exhibit the same upregulation under hypoxic conditions. HIF-1 α was a key gene in the hypoxia and glycolysis signaling pathways. mTOR acts as a crucial upstream regulator of HIF-1 α , participating in the hypoxia signaling pathway and regulating cellular energy metabolism. Interestingly, in GP73-deficient T cells, mTOR activity was reduced following hypoxic treatment (online supplemental figure S4A). In contrast, both exogenous overexpression of HIF-1 α and pharmacological activation of mTOR were able to restore glycolysis in the cells under hypoxic conditions (online supplemental figure S4B–D). To investigate whether GP73 regulated the expression of HIF-1 α and its downstream genes, we cultured WT and GP73-deficient T cells under both normoxic (21% O₂) and hypoxic conditions. After T cells activated, those lacking GP73 displayed impaired expression of HIF-1 α and its downstream gene VEGF-A (figure 6G, H). Moreover, the deletion of GP73 impaired the expression of genes related to glycolytic metabolism, including LDHA and PDK1 (figure 6D–G). Based on the above results, we proposed that GP73 knockout in T cells is associated with restricted

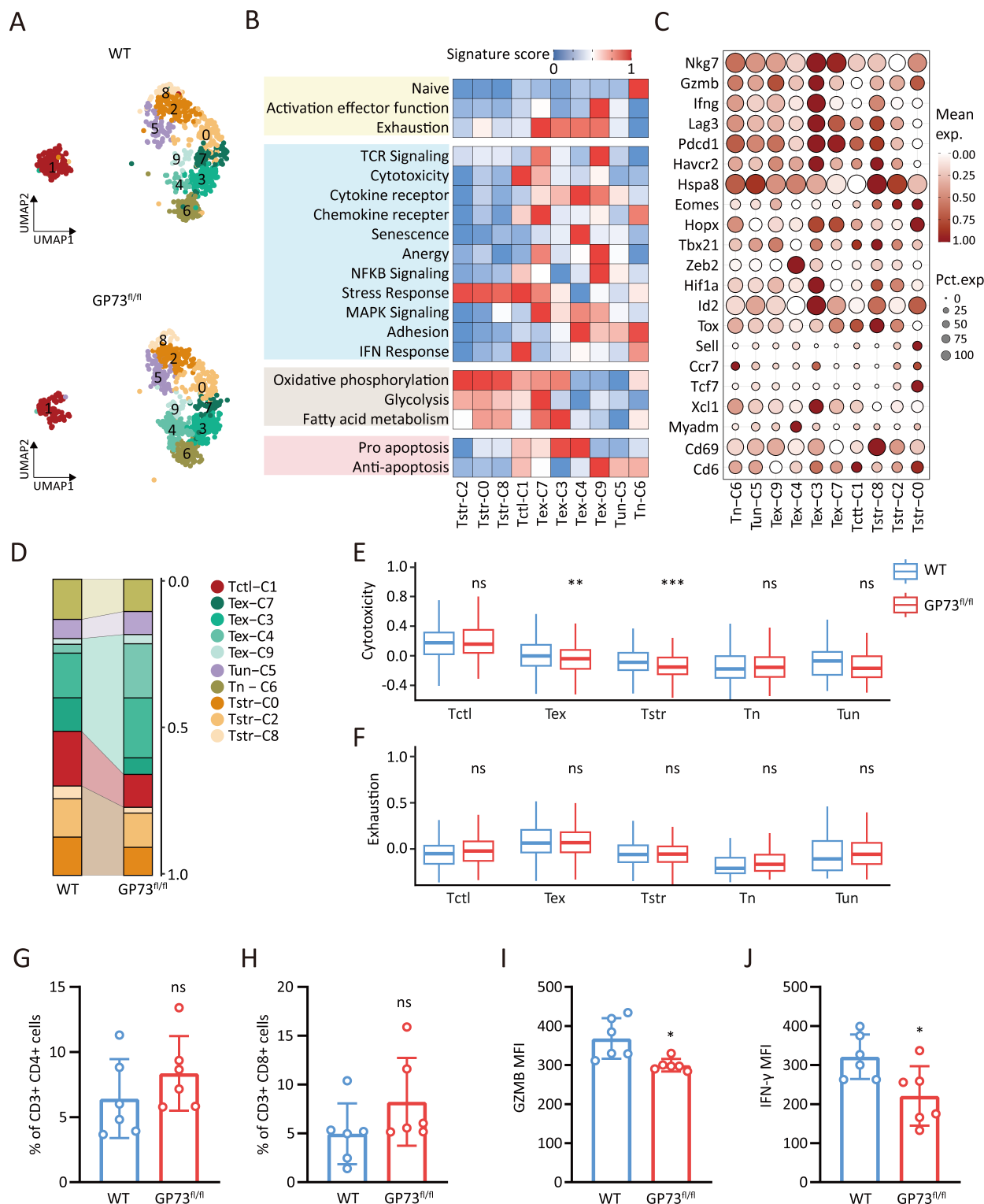


Figure 4 Reduced cytotoxicity of GP73-deficient T cells. (A) UMAP plots of scRNA-seq data from WT and GP73^{fl/fl} T cells, all T cells are divided into 10 clusters. (B) The scores of signature calculated by the mean expression of gene sets related to these T cell status, and all T-cell subsets were defined based on scores. (C) Expression levels of some cytokines, immune checkpoints, and glycolysis-related genes in various T-cell subsets. (D) The histogram shows the proportion of each T-cell subset. (E, F) Box plots show the scores associated with cytotoxicity (E) and exhaustion (F) for each subset of CD8⁺ T cells (Tctl, Tex, Tstr, Tn and Tun) in WT and GP73^{fl/fl}. (G) Flow cytometry analysis tumor-infiltrating T cells from WT and GP73^{fl/fl} mice. Bar graph showing the proportion of CD3⁺CD4⁺ T cells (n=6, error bars represent SD). (H) Bar graph showing the proportion of CD3⁺CD8⁺ T cells (n=6, error bars represent SD). (I) Bar graph representing the MFI of GZMB in CD3⁺CD8⁺ T cells (n=6, error bars represent SD). (J) Bar graph representing the MFI of IFN- γ in CD3⁺CD8⁺ T cells (n=6, error bars represent SD). ***p<0.001, **p<0.01, *p<0.05. GP73, Golgi protein 73; ns, not significant; scRNA-seq, single-cell RNA sequencing; UMAP, uniform manifold approximation and projection; WT, wildtype.

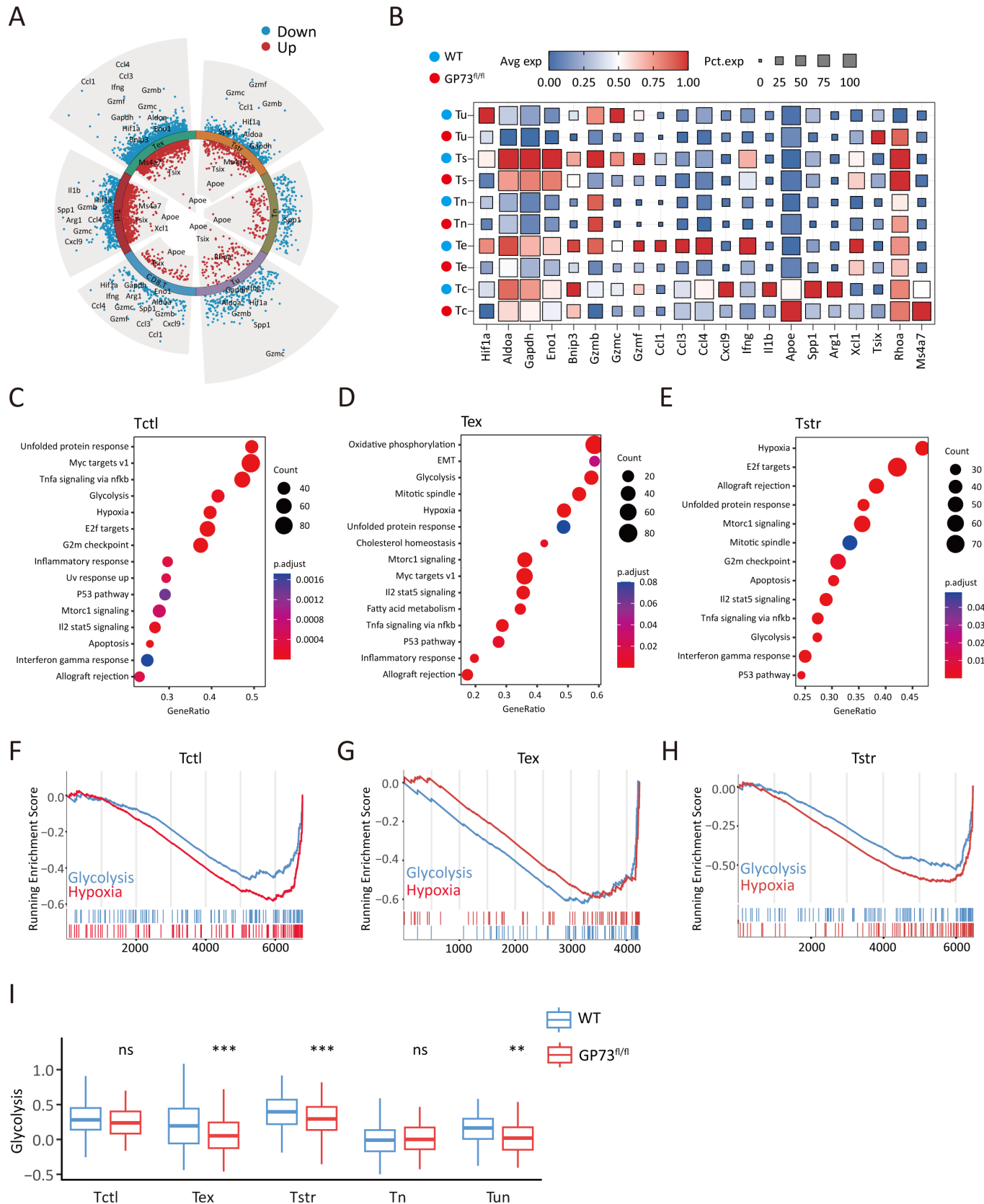


Figure 5 Glycolytic pathway inhibited in GP73-deficient T cells. (A) Volcano plot showing genes differentially expressed in indicated clusters. (B) Z-score normalized mean expression of selected T-cell function and metabolism associated genes in indicated clusters of WT and GP73^{fl/fl}. (C–E) Bubble chart of KEGG pathway enrichment analysis based on Tct1 (C), Tex (D) and Tstr (E) clusters. (F–H) GSEA of hypoxia and glycolysis signature in GP73^{fl/fl} versus WT from indicated clusters. (I) Box plots show the scores associated with glycolysis for indicated subset of T cells in WT and GP73^{fl/fl}. GP73, Golgi protein 73; GSEA, gene set enrichment analysis; KEGG, Kyoto Encyclopedia of Genes and Genomes; WT, wildtype.

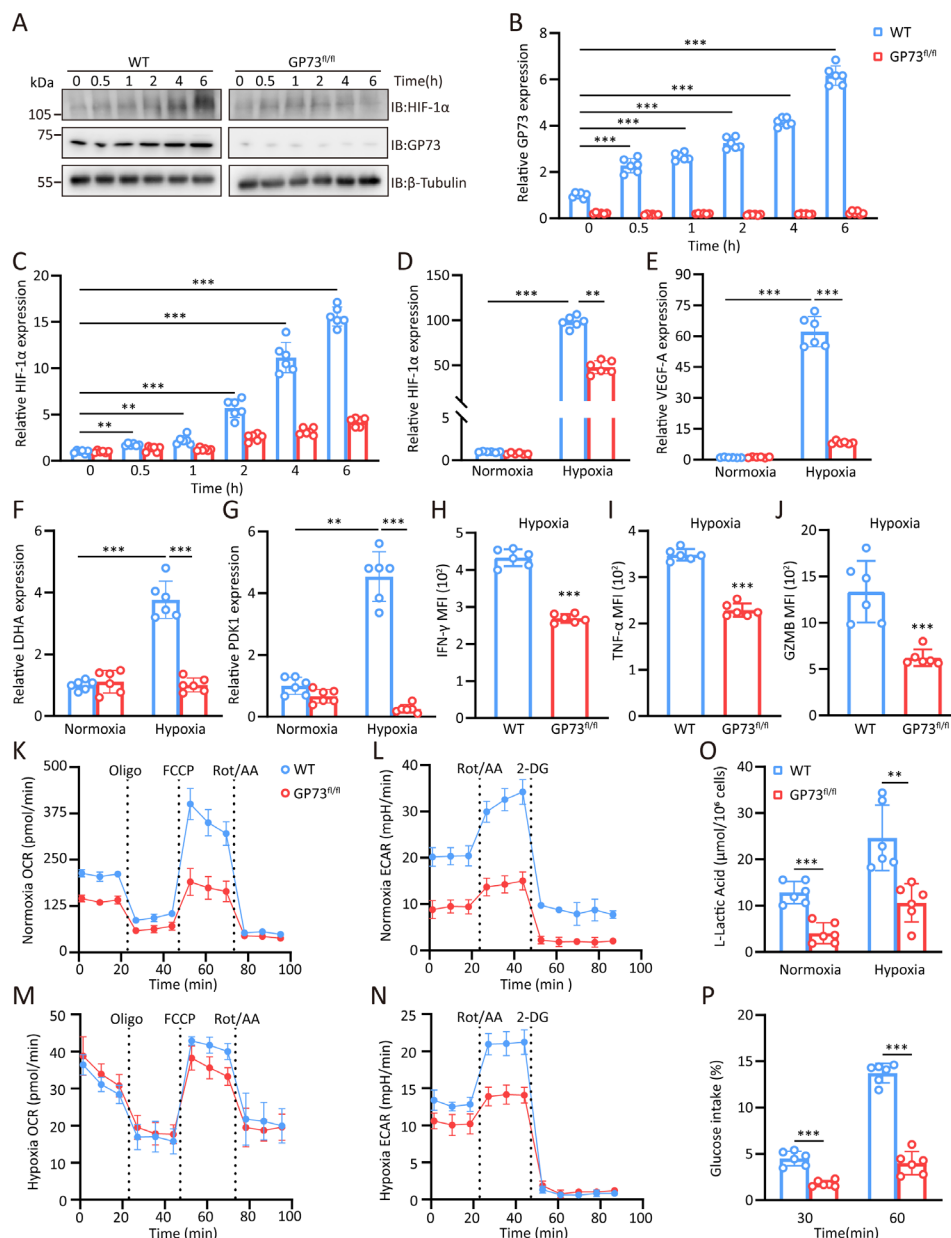


Figure 6 Genetic deletion of GP73 leads to restrain glycolysis by regulating mTOR-HIF-1 α signaling. (A) T cells from WT and GP73^{fl/fl} were isolated, activated, expanded for 3 days in the presence of IL-2, and incubated in a hypoxic chamber for 0, 0.5, 1, 2, 4 or 6 hour before samples were harvested. The levels of the indicated proteins were determined by immunoblotting. (B, C) qRT-PCR showing GP73 (B) and HIF-1 α (C) expression in activated T cells from WT and GP73^{fl/fl} after incubated in a hypoxic chamber for indicated time points. (n=6, error bars represent SD). (D–G) The levels of HIF-1 α (D), VEGF-A (E), LDHA (F) and PDK1 (G) in activated T cells from WT and GP73^{fl/fl} after cultured for 24 hours under normoxic versus hypoxic conditions (n=6, error bars represent SD). (H–J) MFI of IFN- γ (H), TNF- α (I) and GZMB (J) in activated CD3+CD8+ T cells from WT and GP73^{fl/fl} measured by flow cytometry after incubated in a hypoxic conditions (n=6, error bars represent SD). (K–N) ECAR and OCR of activated T cells were measured by flux analysis under the indicated conditions (Oligo: oligomycin, an antifungal antibiotic, inhibiting mitochondrial complex V in the respiratory chain blocks oxidative phosphorylation and electron transfer; FCCP: trifluoromethoxy carbonyl cyanide phenylhydrazine, a mitochondrial uncoupler that disrupts the proton gradient and mitochondrial membrane potential; Rot/AA: rotenone and antimycin, rotenone is an inhibitor of mitochondrial complex I, while antimycin A inhibits mitochondrial complex III. Both agents can effectively shut down mitochondrial respiration, allowing for the calculation of oxygen consumption driven by non-mitochondrial respiration; 2-DG: 2-deoxy-D-glucose, competitively binds to hexokinase in the glycolytic pathway, thereby inhibiting glycolysis; n=5 per group, error bars represent SD). (O) Supernatants of activated T cells from WT and GP73^{fl/fl} were measured for L-lactic acid levels (n=6, error bars represent SD). (P) The glucose uptake rate of T cells from WT and GP73^{fl/fl} was determined by flow cytometry with 2-NBDG under hypoxic conditions, and positive cell percentage was recorded in 30 and 60 minutes (n=6, error bars represent SD). Grouped data were assessed by two-way ANOVA for multiple comparisons with Sidak correction. ***p<0.001, **p<0.01, *p<0.05. ANOVA, analysis of variance; ECAR, extracellular acidification rate; GP73, Golgi protein 73; HIF-1 α , hypoxia-inducible factor 1 α ; OCR, oxygen consumption rate; ns, not significant.

expression of glycolysis-related genes. Since the TME was often hypoxic and glycolysis serves as the primary energy source for tumor-infiltrating T cells, we hypothesized that the knockout of GP73 impairs T-cell cytotoxicity by affecting glycolysis. To test this, we measured the cytokine levels secreted by T cells after hypoxic treatment. As expected, the hypoxic GP73-deficient CD8⁺ T cells exhibited reduced secretion of IFN- γ , TNF- α and GZMB, further supporting our hypothesis (figure 6H–J, online supplemental figure S5A–C). Simultaneously, we used seahorse assays to directly study the impact of GP73 deficiency on T-cell energy metabolism. Our study demonstrated that knockout GP73 in T cells significantly impacts cellular energy metabolism. Under both normoxic and hypoxic condition, it led to substantial inhibition of glycolysis. Therefore, we further hypothesized that GP73-deficient T cells are unable to obtain sufficient energy within the hypoxic tumor microenvironment, which severely compromised their antitumor capabilities (figure 6K–N); additional details are available in online supplemental figure S5D–G. Moreover, it influenced the glucose intake rate and L-lactic acid production. GP73-deficient T cells significantly reduced the glucose intake rate and L-lactic acid secretion (figure 6O, P). These results collectively indicated that GP73 plays a pivotal role in regulating the function of cytotoxic T cells by modulating HIF-1 α -mediated metabolic pathways.

Ectopic expression of GP73 in T cells restores glycolysis and cytotoxicity

Because the knockout of GP73 leads to decreased T-cell glycolysis, we next investigated whether the ectopic expression of GP73 in GP73-deficient T cells can restore T-cell glycolysis. We developed a lentivirus that expresses high levels of GP73 in mice, allowing for stable expression of GP73 in T cells (figure 7A). We subsequently induced the ectopic expression of GP73 in GP73-deficient T cells (hereafter, GP73^{fl/fl} + pCDH-GP73), a method that does not affect cell proliferation (online supplemental figure S6A). Our immunoblotting analyses revealed that ectopic GP73 can restore HIF-1 α expression in GP73^{fl/fl} + pCDH-GP73 T cells and that the levels of GP73 and HIF-1 α were continuously increased under hypoxic conditions (figure 7B); however, the transcription level of GP73 did not change (figure 7C). Importantly, after culture under hypoxic conditions, GP73 overexpression promoted the expression of HIF-1 α , VEGF-A, LDHA and PDK1 (figure 7D–G) and promoted the production of L-lactic acid (figure 7H). We then investigated whether ectopic GP73 expression could restore glucose intake in GP73-deficient T cells. We cultured GP73^{fl/fl} + pCDH-GP73 T cells under hypoxic conditions for 30 and 60 min. As shown, the glucose intake rate of the GP73^{fl/fl} + pCDH-GP73 T cells was significantly improved (figure 7I). Next, we used T-cell adoptive therapy to evaluate the effect of ectopic expression of GP73 on the antitumor activity of CD8⁺ T cells. WT mice were inoculated with MC38-OVA, followed by adoptive transfer of OT-1 CD8⁺T cells or GP73-overexpressing OT-1 CD8⁺T

cells (hereafter, OT-1^{GP73}); the experimental methods are shown in figure 7J. Eight days after the T-cell injection, the subcutaneous tumors were harvested on sacrifice. Importantly, adoptive transfer of OT-1^{GP73} led to a significant delay in tumor growth (figure 7K, L). Additionally, in the in vitro cytotoxicity assays, silencing GP73 expression in OT-1 CD8⁺ T cells (hereafter, OT-1^{shGP73}) was associated with reduced cytotoxicity (figure 7M). Moreover, the release of cytokines IFN- γ , TNF- α and GZMB was significantly decreased (figure 7N–P); the silencing efficiency of GP73 is shown in online supplemental figure S6B; specific microscopy images are shown in online supplemental figure S6C. These findings highlighted a potential approach to enhancing the antitumor efficacy of therapeutic CD8⁺ T cells through ectopic expression of GP73 and suggested that the efficacy of clinical tumor immunotherapy may be related to the expression level of GP73 in T cells.

GP73 upregulation in T cells of patients with lung cancer with partial response to anti-PD-1 therapy

In our previous experiments, we reported that GP73 expression levels were significantly elevated in the peripheral blood T cells of patients with cancer compared with those of healthy individuals (online supplemental figure S7A). To investigate the potential correlation between tumor immunotherapy efficacy and GP73 expression levels in T cells, we collected clinical samples from patients with lung cancer receiving anti-PD-1 immunotherapy (figure 8A). On the basis of the Response Evaluation Criteria in Solid Tumors (RECIST), as well as patients' baseline clinical information (online supplemental table S1), treatment cycles, and therapeutic outcomes, we categorized patients into partial response and stable disease groups (figure 8B, C). After peripheral blood T cells were isolated from these patients, we focused on examining the differences in GP73 expression between the two groups (online supplemental figure S7B). Notably, compared with those in patients with stable disease, we observed a substantial increase in GP73 levels in patients who showed a partial response to anti-PD-1 treatment (figure 8D). These findings revealed that upregulation of GP73 in T cells is associated with better anti-PD-1 efficacy in patients, suggesting a correlation between GP73 and anti-PD-1 efficacy.

DISCUSSION

Hypoxia is a prominent feature of solid tumors and not only causes tumor cell metabolic reprogramming, known as the Warberg effect, but also promotes metabolic reprogramming of tumor-infiltrating immune cells, such as a weakened inflammatory response and immune effector function.^{33–35} Moreover, the hypoxic TME prompts many cells to express hypoxia-related transcription factors, such as cytokine-induced HIF-1 α , so that cells can adapt to this hypoxic environment.³⁶ Therefore, studying the effect of

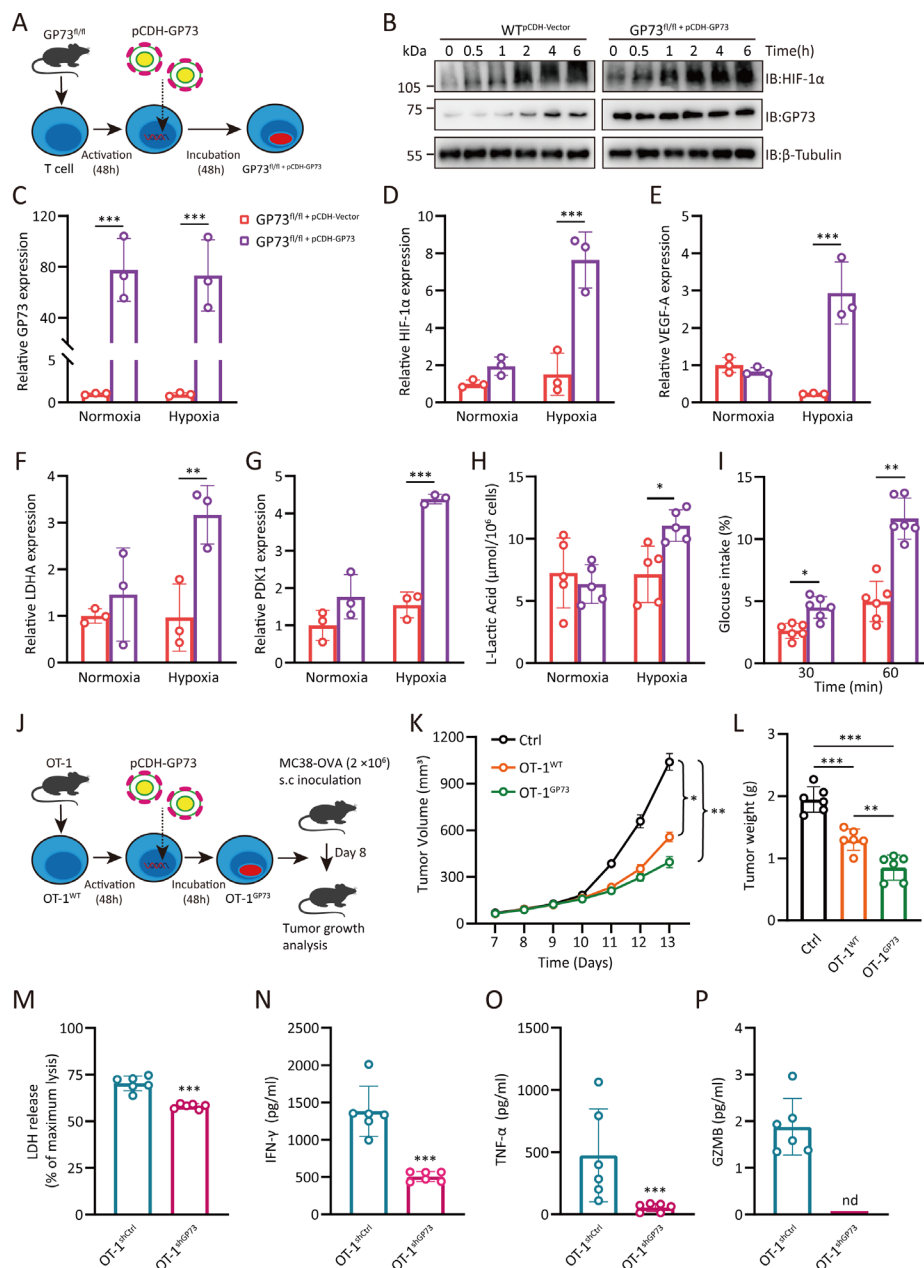


Figure 7 Exogenous GP73 expression restores glycolysis and cytotoxicity in T cells. (A) T cells from GP73^{fl/fl} were activated for 48 hours before infection with lentiviral. After 48 hours of incubation, ectopic GP73 was highly expressed in T cells (GP73^{fl/fl} + pCDH-GP73). (B) The protein levels of GP73 and HIF-1α in WT^{pCDH-Vector} and GP73^{fl/fl} + pCDH-GP73 cells were determined by immunoblotting after incubation at the indicated time points in a hypoxic conditions. (C–G) The levels of GP73 (C), HIF-1α (D), VEGF-A (E), LDHA (F) and PDK1 (G) in activated GP73^{fl/fl} + pCDH-Vector and GP73^{fl/fl} + pCDH-GP73 cells after cultured for 24 hours under normoxic vs hypoxic conditions (n=3, error bars represent SD). (H) Supernatants of activated GP73^{fl/fl} + pCDH-Vector and GP73^{fl/fl} + pCDH-GP73 cells were measured for L-lactic acid levels (n=5, error bars represent SD). (I) The glucose uptake rate of GP73^{fl/fl} + pCDH-Vector and GP73^{fl/fl} + pCDH-GP73 cells was determined by flow cytometry with 2-NBDG under hypoxic conditions (n=6, error bars represent SD). (J) Adoptive immunotherapy schematic diagram. CD8⁺T cells were isolated from the spleen of OT-1 mice and then infected with pCDH-vector (OT-1^{WT}) or pCDH-GP73 (OT-1^{GP73}). After 8 days of subcutaneous injection of MC38-OVA (2×10⁶ cells per mouse), both OT-1^{WT} and OT-1^{GP73} cells (1×10⁶ cells per mouse) were intravenously administered to the mice to inhibit tumor growth (n=6). (K) Growth curves of subcutaneous MC38-OVA tumors in Ctrl (black), OT-1^{WT} (orange) and OT-1^{GP73} (green); statistical analysis was performed by two-way ANOVA with Dunnett-t correction for multiple comparisons; Ctrl: control group, intravenous injection of PBS (100 μl per mouse); error bars represent SD. (L) MC38-OVA tumor weights on day 14 of the experiment (error bars represent SD). (M) Bar graph displays the levels of LDH release in the cell supernatant after target cell killing by the OT-1^{shCtrl} and OT-1^{shGP73} groups (n=6, error bars represent SD). (N–P) Bar graph shows the concentrations of IFN-γ (N), TNF-α (O) and GZMB (P) released into the supernatant after target cell killing by the OT-1^{shCtrl} and OT-1^{shGP73} groups (n=6, error bars represent SD). Grouped data were assessed by two-way ANOVA for multiple comparisons with Sidak correction. ***p<0.001, **p<0.01, *p<0.05. ANOVA, analysis of variance; GP73, Golgi protein 73; HIF-1α, hypoxia-inducible factor 1α; LDH, lactate dehydrogenase; ns, not significant.

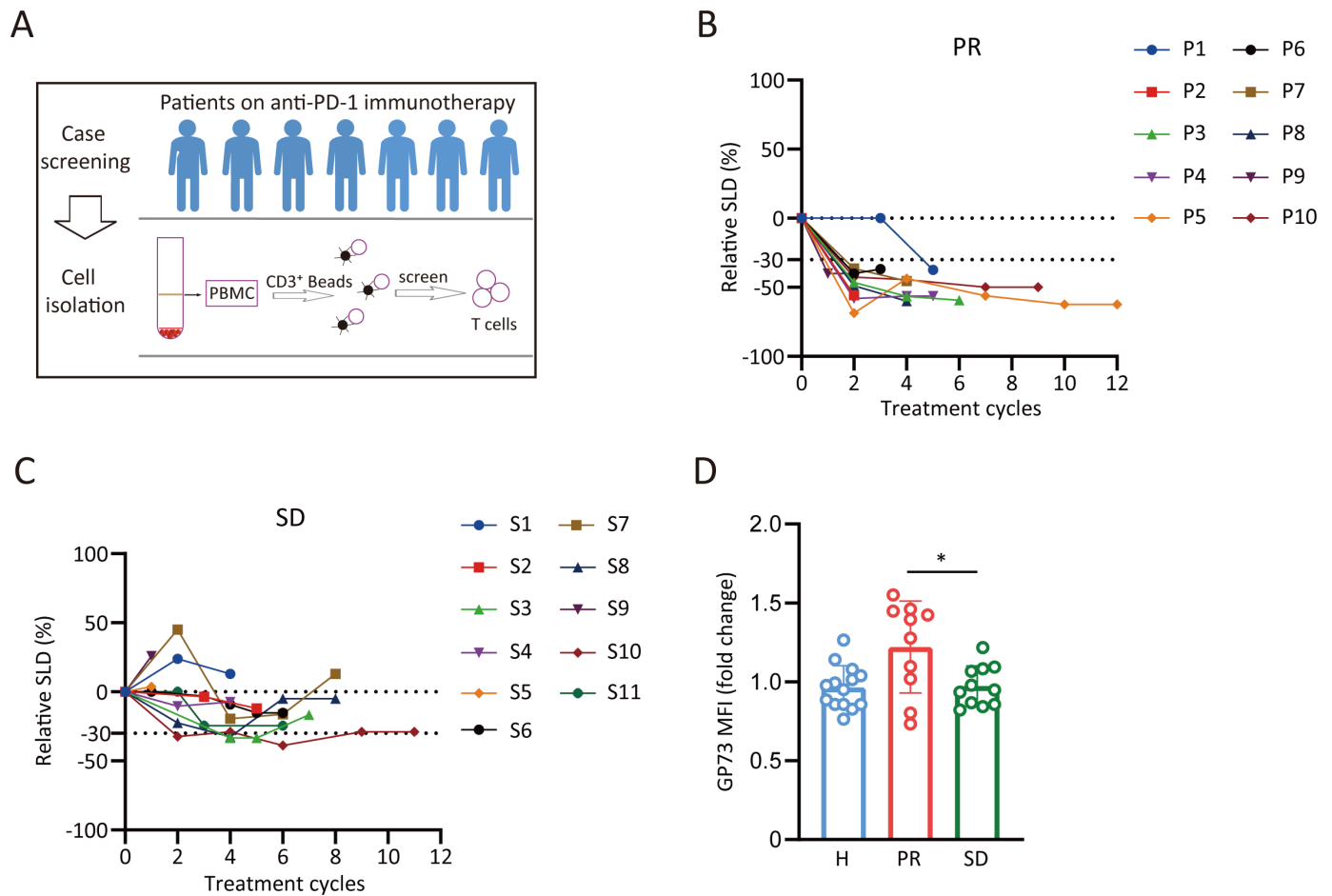


Figure 8 Efficacy of anti-PD-1 therapy is correlated with T-cell GP73. (A) Workflow of the experimental design including clinical sample collection and T-cell isolation. (B–C) Correlation analysis of SLD and the anti-PD-1 treatment cycles of patients from PR and SD groups. (D) Bar graph showing relative MFI of GP73 in T cells isolated from indicated groups (n=10–11, error bars represent SD). *p<0.05. GP73, Golgi protein 73; H, Healthy; PR, partial response; SD, stable disease; SLD, tumor lesion sum of the longest diameters.

the hypoxic environment on tumor-infiltrating immune cells may lead to a cure for cancer.

Hypoxia promotes cellular metabolism from oxidative phosphorylation to glycolysis; therefore, most cells in the TME rely on glycolysis as the main mode of energy.³⁷ HIF-1 α is not only a key characteristic factor of hypoxia signaling but also a key regulator of glycolysis, and the expression of HIF-1 α in cells is particularly important for the physiological function of cells in a hypoxic environment. Here, we found that GP73 in T cells was involved in regulating the expression of HIF-1 α , especially in a hypoxic environment, and that the expression of GP73 in T cells was positively correlated with the expression of HIF-1 α . Undoubtedly, these results provided a key evidence that T-cell GP73 can regulate cellular glycolysis under hypoxia.

GP73 was first found to be highly expressed in the liver tissue of patients with giant cell hepatitis, and subsequent studies revealed that GP73 was expressed at very low levels in normal hepatocytes but was significantly increased in the livers of patients with acute or chronic liver disease.^{38,39} As a type II transmembrane glycoprotein located in the

Golgi apparatus, GP73 maintains the normal structure of the Golgi apparatus and assists in protein function; therefore, GP73 may be involved in the transport of intracellular proteins. GP73 plays different roles in various immune cells. Previous studies have demonstrated that elevated levels of GP73 in TAMs can induce CD8⁺ T-cell suppression by promoting PD-L1 stabilization and facilitating the transport of PD-L1 into TAMs via an exosome-dependent mechanism.²⁵ Additionally, GP73 has been shown to activate ER stress in neighboring macrophages, triggering the release of cytokines and chemokines that contribute to the TAM phenotype.²⁴ In our study, we used GP73^{fl/fl} mice to investigate the intrinsic effects of GP73 on T-cell function. We observed that GP73 expression increased in response to T-cell activation, suggesting that GP73 may play a critical role in modulating T-cell effector functions. These findings provided important insights into the role of GP73 in immune regulation within the TME.

We subsequently wanted to evaluate the consequences of T-cell deletion of GP73. T cells play an important role in antitumor immunity, and clinical tumor immunotherapy

also fights tumors by enhancing the effector function of T cells. To investigate the impact of GP73 on T cells following T-cell deficiency, we established mouse tumor models using three different immunogenic tumor cell lines. The results indicated that the absence of GP73 in T cells accelerated tumor growth, particularly in highly immunogenic tumor cell lines, and increased mouse mortality. However, the growth of the low-immunogenic LLC tumor cells was not affected, although mortality still occurred in the knockout mice. This may be due to the ability of LLC tumors to induce specific T-cell responses, while GP73 knockout can directly impair the cytotoxic activity of CD8⁺ T cells, potentially affecting the functions of various T-cell subsets, including regulatory T cells. This, in turn, impacted the composition and function of immune cells in the TME, ultimately affecting mouse survival. These findings warrant further investigation. According to previous studies, high expression of GP73 often predicted disease progression, especially in HCC, and some scholars believed that the combination of GP73 and AFP was more valuable for predicting HCC than AFP alone is.⁴⁰ These findings have greatly increased our interest in this topic and prompted us to investigate the mechanisms by which GP73 affects T-cell function.

Single-cell sequencing provides a complete picture of the composition of tumor-infiltrating immune cells, and we were eager to look for compositional differences in different immune cells, but GP73 knockout in T cells was not associated with the proportion of CD4⁺ or CD8⁺ T cells. Many interesting results have shown that CD8⁺ T cells are the main population involved in antitumor activity. CD4⁺ T cells are involved in directing the immune response and can also be used by tumor cells to achieve immune escape. Therefore, we focused our analysis on CD8⁺ T-cell subsets, and interestingly, the proportion of exhausted CD8⁺ T cells increased and the proportion of cytotoxic CD8⁺ T cells decreased. Importantly, this depletion was not dependent on changes in immune checkpoints but rather is due to an insufficient glycolytic energy supply. We found that HIF-1 α was underexpressed in almost all CD8⁺ T-cell subsets; therefore, our study further explored the effect of GP73 on HIF-1 α and elucidated the underlying regulatory mechanisms involved.

HIF-1 α is expressed in various cell types, including T cells, particularly within the hypoxic environment of solid tumors. While several mechanisms can induce HIF-1 α expression, limited research has been conducted on HIF-1 α expression in the hypoxic tumor environment, specifically in T cells. Our findings showed that T cells expressed GP73 at the transcriptional and protein levels, and activation was accompanied by increased GP73 and HIF-1 α expression. These findings increased our confidence in the conclusion that GP73 regulated HIF-1 α . Studies have shown that knockdown of HIF-1 α results in defective T-cell differentiation and reduced antitumor ability, underscoring the importance of HIF-1 α in tumor progression.¹⁴ Proteins that play a key role in CTL-mediated tumor rejection are thought to be associated

with HIF-1 α .⁴¹ On the other hand, ablation of HIF-1 α in T cells suppressed the production of cytokines such as IFN- γ , TNF- α and GZMB.¹⁴ Our results indicated that GP73-deficient T cells exhibited an impaired HIF-1 α -driven transcriptional program and glycolysis under hypoxic conditions, which impacted effector function. Furthermore, we demonstrated that GP73 was vital for controlling effector cell function. Restoring GP73 levels in GP73-deficient T cells can promote cellular glycolysis, and ectopic high expression of GP73 can enhance the antitumor function of T cells. While HIF-1 α regulated the expression of costimulatory and checkpoint receptors, the expression of PD-1 is VHL dependent, not VHL/HIF-1 α /HIF-2 α dependent, suggested that PD-1 downregulation was not directly attributed to HIF-1 α .^{14 42} Interestingly, exhaustion-related receptors regulated by HIF-1 α remained unchanged in GP73-deficient T cells, indicating that GP73 influences T-cell function partly through regulating HIF-1 α .

To investigate the mechanism by which GP73 regulates HIF-1 α , we examined the expression of upstream regulatory factors of HIF-1 α during hypoxia in T cells. As a key physiological signaling regulator, the expression levels of mTOR and its phosphorylated form were closely monitored. Previous studies have confirmed that mTORC1 regulated GP73 expression in cell lines.⁴³ Additionally, our experiments demonstrated that GP73 knockout significantly reduced mTOR activity in T cells under hypoxic conditions. Together with prior findings, these results indicated a synergistic expression effect between activated mTOR and GP73 levels. Seahorse assay results further supported that GP73 knockout significantly inhibits mTOR activity, as characterized by the stability of pharmacological activation of mTOR to restore ECAR under hypoxic conditions. Therefore, we hypothesized that GP73 knockout inhibited HIF-1 α -driven glycolysis by reducing mTOR activity.

To further validate our findings, we enrolled a cohort of patients with tumor receiving anti-PD-1 therapy in this study. On the basis of clinical recommendations, the patients were stratified into two groups: those who exhibited a partial response to PD-1 therapy and those who tolerated the treatment. The results revealed that the GP73 levels in the T cells of patients who achieved a partial response to PD-1 treatment were significantly elevated. These data suggested that GP73 expression in T cells was associated with the response to anti-PD-1 therapy. In the future, more patients should be recruited to study the relationship between GP73 and HIF-1 α and to clarify the function of GP73.

In conclusion, our study demonstrates a novel cancer treatment strategy that is independent of immune checkpoints but rather involves increasing the level of cellular glycolysis and adapting cells to the hypoxic TME, thereby achieving tumor suppression, which provides strong support for the immunotherapy. We demonstrated that GP73 was an important regulator of T-cell effector

responses in the TME and that the control of HIF-1 α in effector T cells through GP73 contributed to T-cell tumor suppression. To translate these findings into a preclinical human context, we generated a vector for expressing GP73 in T cells. Notably, in an in vivo xenograft model, the expression of mouse GP73 significantly enhanced the cytotoxic effect of CD8 $^{+}$ T cells on tumors. These results suggested that GP73 may represent a key and innovative addition to the arsenal of CAR-T-cell therapy.

CONCLUSIONS

In summary, our research demonstrated that GP73 regulated the glycolytic level of T cells under hypoxia by modulating HIF-1 α , thereby influencing the antitumor function of T cells within the TME. These findings suggested that targeting GP73 could be a novel therapeutic strategy for improving the prognosis and treatment of patients receiving clinical tumor immunotherapy.

Author affiliations

¹Department of Clinical Laboratory, The Third Medical Center of Chinese PLA General Hospital, Beijing, Beijing, China

²Clinical Diagnosis Laboratory, Beijing Tiantan Hospital Affiliated to Capital Medical University, Beijing, Beijing, China

³Department of Basic Medical Sciences, 960th Hospital of People's Liberation Army Joint Logistic Support Force, Jinan, Shandong, China

⁴Department of Clinical Laboratory, The 969th Hospital of PLA, Hohhot, Inner Mongolia, China

⁵Department of Genetic Engineering, Academy of Military Medical Sciences, Beijing, Beijing, China

⁶Department of Pharmacy, PLA General Hospital Medical Supplies Center Department of Pharmacy, Beijing, Beijing, China

⁷Beijing Hotgen Biotech Co., Ltd, Beijing, Beijing, China

⁸National-Local Joint Engineering Research Center of Biodiagnosis & Biotherapy, Second Affiliated Hospital of Xi'an Jiaotong University, Xi'an, Shaanxi, China

⁹Department of Gastroenterology, The Fifth Medical Center of Chinese PLA General Hospital, Beijing, Beijing, China

Acknowledgements We would like to thank professor Guojun Zhang's team from the Clinical Diagnosis Laboratory of Beijing Tiantan Hospital for their expert technical assistance.

Contributors XY, HZ, YC, XM, MM and CW contributed to the conception, design and writing of the paper; XY, HZ, YC, CW, JL, CF, LH and XY drafted the manuscript; JL, ML, LW, XZ, YZ and QG revised the manuscript; LL, CD and HS collected clinical samples; LS, XH, YZ, HS, NJ, DZ, YL and YW acquired and analyzed the data; and XY, HZ, YC, CW, JL, CF and XM interpreted the data. Author acting as guarantor: XY. All the authors discussed the results and reviewed the manuscript, both online and in person.

Funding This work was supported by the National Natural Science Foundation of China (grant nos. 81972696), the Beijing Nova Program (grant no. 20240484702) and Natural Science Foundation of Shandong Province (grant no. ZR2023MH370).

Competing interests None declared.

Patient consent for publication Not applicable.

Ethics approval This study involves human participants and was approved by the Ethics Committee of the Chinese PLA General Hospital (KY2021-009-01). Participants gave informed consent to participate in the study before taking part.

Provenance and peer review Not commissioned; externally peer reviewed.

Data availability statement Data are available in a public, open access repository. Data are available upon reasonable request. The data and corresponding analysis code have deposited in Zenodo repository (<https://doi.org/10.5281/zenodo.14045439>). Digital source data are provided in source data files and, where reasonable, at the discretion of the corresponding author.

Supplemental material This content has been supplied by the author(s). It has not been vetted by BMJ Publishing Group Limited (BMJ) and may not have been peer-reviewed. Any opinions or recommendations discussed are solely those of the author(s) and are not endorsed by BMJ. BMJ disclaims all liability and responsibility arising from any reliance placed on the content. Where the content includes any translated material, BMJ does not warrant the accuracy and reliability of the translations (including but not limited to local regulations, clinical guidelines, terminology, drug names and drug dosages), and is not responsible for any error and/or omissions arising from translation and adaptation or otherwise.

Open access This is an open access article distributed in accordance with the Creative Commons Attribution Non Commercial (CC BY-NC 4.0) license, which permits others to distribute, remix, adapt, build upon this work non-commercially, and license their derivative works on different terms, provided the original work is properly cited, appropriate credit is given, any changes made indicated, and the use is non-commercial. See <http://creativecommons.org/licenses/by-nc/4.0/>.

ORCID iDs

Jialong Liu <http://orcid.org/0009-0004-3482-9869>

Yuan Cao <http://orcid.org/0000-0002-2681-8711>

REFERENCES

- Patel S, Burga RA, Powell AB, *et al.* Beyond CAR T Cells: Other Cell-Based Immunotherapeutic Strategies Against Cancer. *Front Oncol* 2019;9:196.
- Paijens ST, Vledder A, de Bruyn M, *et al.* Tumor-infiltrating lymphocytes in the immunotherapy era. *Cell Mol Immunol* 2021;18:842–59.
- Mishra AK, Malonia SK. Advancing cellular immunotherapy with macrophages. *Life Sci* 2023;328:121857.
- Badalamenti G, Fanale D, Incorvaia L, *et al.* Role of tumor-infiltrating lymphocytes in patients with solid tumors: Can a drop dig a stone? *Cell Immunol* 2019;343:103753.
- Labiano S, Palazon A, Melero I. Immune response regulation in the tumor microenvironment by hypoxia. *Semin Oncol* 2015;42:378–86.
- Kopecka J, Salaroglio IC, Perez-Ruiz E, *et al.* Hypoxia as a driver of resistance to immunotherapy. *Drug Resist Updat* 2021;59:100787.
- Arnaiz E, Harris AL. Role of Hypoxia in the Interferon Response. *Front Immunol* 2022;13:821816.
- Neildez-Nguyen TMA, Bigot J, Da Rocha S, *et al.* Hypoxic culture conditions enhance the generation of regulatory T cells. *Immunology* 2015;144:431–43.
- Wu Q, You L, Nepovimova E, *et al.* Hypoxia-inducible factors: master regulators of hypoxic tumor immune escape. *J Hematol Oncol* 2022;15:77.
- Phan AT, Goldrath AW. Hypoxia-inducible factors regulate T cell metabolism and function. *Mol Immunol* 2015;68:527–35.
- Palazon A, Goldrath AW, Nizet V, *et al.* HIF transcription factors, inflammation, and immunity. *Immunity* 2014;41:518–28.
- Wan J, Wu W, Che Y, *et al.* Low dose photodynamic-therapy induce immune escape of tumor cells in a HIF-1 α dependent manner through PI3K/Akt pathway. *Int Immunopharmacol* 2015;28:44–51.
- Doedens AL, Phan AT, Stradner MH, *et al.* Hypoxia-inducible factors enhance the effector responses of CD8 $^{+}$ T cells to persistent antigen. *Nat Immunol* 2013;14:1173–82.
- Palazon A, Tyrakis PA, Macias D, *et al.* An HIF-1 α /VEGF-A Axis in Cytotoxic T Cells Regulates Tumor Progression. *Cancer Cell* 2017;32:669–83.
- Miska J, Lee-Chang C, Rashidi A, *et al.* HIF-1 α Is a Metabolic Switch between Glycolytic-Driven Migration and Oxidative Phosphorylation-Driven Immunosuppression of Tregs in Glioblastoma. *Cell Rep* 2019;27:226–37.
- Wu H, Zhao X, Hochrein SM, *et al.* Mitochondrial dysfunction promotes the transition of precursor to terminally exhausted T cells through HIF-1 α -mediated glycolytic reprogramming. *Nat Commun* 2023;14:6858.
- Liikanen I, Lauhan C, Quon S, *et al.* Hypoxia-inducible factor activity promotes antitumor effector function and tissue residency by CD8 $^{+}$ T cells. *J Clin Invest* 2021;131:e143729.
- Hu L, Li L, Xie H, *et al.* The Golgi localization of GOLPH2 (GP73/GOLM1) is determined by the transmembrane and cytoplasmic sequences. *PLoS ONE* 2011;6:e28207.
- Yang X, Wu F, Chen J, *et al.* GP73 regulates Hepatic Steatosis by enhancing SCAP-SREBPs interaction. *Sci Rep* 2017;7:14932.
- Song Q, He X, Xiong Y, *et al.* The functional landscape of Golgi membrane protein 1 (GOLM1) phosphoproteome reveal GOLM1

- regulating P53 that promotes malignancy. *Cell Death Discov* 2021;7:42.
- 21 Wei S, Dunn TA, Isaacs WB, *et al.* GOLPH2 and MYO6: putative prostate cancer markers localized to the Golgi apparatus. *Prostate* 2008;68:1387–95.
 - 22 Liu Y, Hu X, Liu S, *et al.* Golgi Phosphoprotein 73: The Driver of Epithelial-Mesenchymal Transition in Cancer. *Front Oncol* 2021;11:783860.
 - 23 Yan J, Zhou B, Guo L, *et al.* GOLM1 upregulates expression of PD-L1 through EGFR/STAT3 pathway in hepatocellular carcinoma. *Am J Cancer Res* 2020;10:3705–20.
 - 24 Wei C, Yang X, Liu N, *et al.* Tumor Microenvironment Regulation by the Endoplasmic Reticulum Stress Transmission Mediator Golgi Protein 73 in Mice. *Hepatology* 2019;70:851–70.
 - 25 Chen J, Lin Z, Liu L, *et al.* GOLM1 exacerbates CD8⁺ T cell suppression in hepatocellular carcinoma by promoting exosomal PD-L1 transport into tumor-associated macrophages. *Signal Transduct Target Ther* 2021;6:397.
 - 26 Peng Y, Zeng Q, Wan L, *et al.* GP73 is a TBC-domain Rab GTPase-activating protein contributing to the pathogenesis of non-alcoholic fatty liver disease without obesity. *Nat Commun* 2021;12:7004.
 - 27 Yado S, Dassa B, Zoabi R, *et al.* Molecular mechanisms underlying the modulation of T-cell proliferation and cytotoxicity by immobilized CCL21 and ICAM1. *J Immunother Cancer* 2024;12:e009011.
 - 28 McGinnis CS, Murrow LM, Gartner ZJ. DoubletFinder: Doublet Detection in Single-Cell RNA Sequencing Data Using Artificial Nearest Neighbors. *Cell Syst* 2019;8:329–37.
 - 29 Korsunsky I, Millard N, Fan J, *et al.* Fast, sensitive and accurate integration of single-cell data with Harmony. *Nat Methods* 2019;16:1289–96.
 - 30 Chu Y, Dai E, Li Y, *et al.* Pan-cancer T cell atlas links a cellular stress response state to immunotherapy resistance. *N Med* 2023;29:1550–62.
 - 31 Feng C, Tao Y, Yu C, *et al.* Integrative single-cell transcriptome analysis reveals immune suppressive landscape in the anaplastic thyroid cancer. *Cancer Gene Ther* 2023;30:1598–609.
 - 32 lanevski A, Giri AK, Aittokallio T. Fully-automated and ultra-fast cell-type identification using specific marker combinations from single-cell transcriptomic data. *Nat Commun* 2022;13:1246.
 - 33 Codony VL, Tavassoli M. Hypoxia-induced therapy resistance: Available hypoxia-targeting strategies and current advances in head and neck cancer. *Transl Oncol* 2021;14:101017.
 - 34 Rickard AG, Palmer GM, Dewhirst MW. Clinical and Pre-clinical Methods for Quantifying Tumor Hypoxia. *Adv Exp Med Biol* 2019;1136:19–41.
 - 35 Masoud GN, Li W. HIF-1 α pathway: role, regulation and intervention for cancer therapy. *Acta Pharm Sin B* 2015;5:378–89.
 - 36 Tam FF, Ning KL, Lee M, *et al.* Cytokine induction of HIF-1 α during normoxia in A549 human lung carcinoma cells is regulated by STAT1 and JNK signalling pathways. *Mol Immunol* 2023;160:12–9.
 - 37 Al Tameemi W, Dale TP, Al-Jumaily RMK, *et al.* Hypoxia-Modified Cancer Cell Metabolism. *Front Cell Dev Biol* 2019;7:4.
 - 38 Kladney RD, Cui X, Bulla GA, *et al.* Expression of GP73, a resident Golgi membrane protein, in viral and nonviral liver disease. *Hepatology* 2002;35:1431–40.
 - 39 Kladney RD, Bulla GA, Guo L, *et al.* GP73, a novel Golgi-localized protein upregulated by viral infection. *Gene* 2000;249:53–65.
 - 40 Pang B-Y, Leng Y, Wang X, *et al.* A meta-analysis and of clinical values of 11 blood biomarkers, such as AFP, DCP, and GP73 for diagnosis of hepatocellular carcinoma. *Ann Med* 2023;55:42–61.
 - 41 Barsoum IB, Smallwood CA, Siemens DR, *et al.* A mechanism of hypoxia-mediated escape from adaptive immunity in cancer cells. *Cancer Res* 2014;74:665–74.
 - 42 Noman MZ, Desantis G, Janji B, *et al.* PD-L1 is a novel direct target of HIF-1 α , and its blockade under hypoxia enhanced MDSC-mediated T cell activation. *J Exp Med* 2014;211:781–90.
 - 43 Chen X, Wang Y, Tao J, *et al.* mTORC1 Up-Regulates GP73 to Promote Proliferation and Migration of Hepatocellular Carcinoma Cells and Growth of Xenograft Tumors in Mice. *Gastroenterology* 2015;149:741–52.